Journal of Medicinal Chemistry

Article

pubs.acs.org/jmc

Structural Dissection of Crotalicidin, a Rattlesnake Venom Cathelicidin, Retrieves a Fragment with Antimicrobial and Antitumor Activity

Claudio Borges Falcao,[†,‡,⊥] Clara Pérez-Peinado,[†,⊥] Beatriz G. de la Torre,[†,⊥] Xavier Mayol,[§] Héctor Zamora-Carreras,[∥] M. Ángeles Jiménez,[∥] Gandhi Rádis-Baptista,[*,†,‡] and David Andreu[*,†]

[†]Departament de Ciències Experimentals i de la Salut, Universitat Pompeu Fabra, 08003 Barcelona, Spain

[‡]Laboratory of Biochemistry and Biotechnology, Institute for Marine Sciences, Federal University of Ceará, 60455-760 Fortaleza, CE, Brazil

[§]Programa de Recerca en Càncer, Institut Hospital del Mar d'Investigacions Mèdiques, 08003 Barcelona, Spain

[∥]Instituto de Química Física "Rocasolano", Consejo Superior de Investigaciones Científicas (CSIC), 28006 Madrid, Spain

Supporting Information

ABSTRACT: In silico dissection of crotalicidin (Ctn), a cathelicidin from a South American pit viper, yielded fragments Ctn[1−14] and Ctn[15−34], which were tested to ascertain to what extent they reproduced the structure and activity of the parent peptide. NMR data showing Ctn to be α-helical at the N-terminus and unstructured at the C-terminus were matched by similar data from the fragments. The peptides were tested against Gram-positive and -negative bacteria and for toxicity against both tumor and healthy cells. Despite its amphipathic α-helical structure, Ctn[1−14] was totally inert toward bacteria or eukaryotic cells. In contrast, unstructured Ctn[15−34] replicated the activity of parent Ctn against Gram-negative bacteria and tumor cells while being significantly less toxic toward eukaryotic cells. This selectivity for bacteria and tumor cells, plus a stability to serum well above that of Ctn, portrays Ctn[15−34] as an appealing candidate for further development as an anti-infective or antitumor lead.

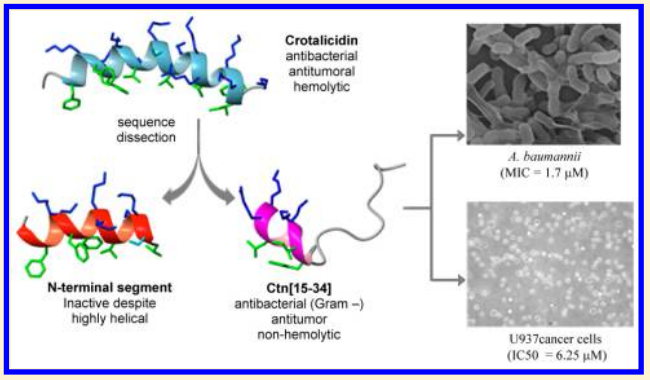

INTRODUCTION

Overuse and misuse of antibiotics have resulted in an ever-growing pattern of microbial resistance at both hospital and community levels that is fast looming into a global health catastrophe.[1−3] Considerable efforts have been dedicated to search and develop new drugs against resistant microorganisms, among which antimicrobial peptides (AMPs) from plants and animals are receiving increasing attention due to their substantial potency, broad spectrum, and distinct mechanism of action. AMPs have been found to be active against a broad range of microorganisms including not only Gram-positive and Gram-negative bacteria but also fungi, protozoa, and viruses.[4−6] AMPs have also shown activity against cancer cells,[7,8] which display a higher variety and density of anionic membrane-bound components (e.g., mucins, sialic acid-containing gangliosides, acidic phospholipids, etc.) than nontumor healthy cells, hence conferring largely cationic AMPs some therapeutic advantage.

Among animal AMPs, the cathelicidins are noteworthy for a wide-ranging species distribution (spanning from primitive hagfish to humans) and broad antimicrobial activity spectra.[9,10] Cathelicidin precursors all share a conserved N-terminal preproregion consisting of a signal peptide sequence and a cathelin (cathepsin L inhibitor) domain, followed by a C-terminal region from which a mature AMP of variable sequence and structure is released by proteolysis (e.g., elastase). In addition, for LL-37 (the only *Homo* cathelicidin reported to date) it has been found that further cleavage by proteases from human sweat generates fragments that retain the activity of the parent AMP.[11] A search for similar processes in cathelicidins from other species has proven experimentally taxing, given restrictions such as limited access to protected species or specimen size, and has therefore been achieved only in virtual form by bioinformatic means.[12,13]

Cathelicidin-related AMPs (CRAMPs) were also found in the venoms of Asian elapid snakes such as king or Chinese cobras or banded krait.[14,15] Like other AMPs, these reptilian CRAMPs act on the membranes of both bacteria, especially Gram-negative,[16] and cancer cells, particularly mouse melanoma.[17] Along similar lines, we recently reported the presence of cathelicidins in South American pit viper snakes.[18] The mature

Received: July 21, 2015
Published: October 14, 2015

DOI: 10.1021/acs.jmedchem.5b01142
J. Med. Chem. 2015, 58, 8553−8563

Table 1. Primary Structure and Physicochemical Properties of Crotalicidin and Fragments

Peptide	Sequence[a]	Molecular mass[b]	Purity[c]	Charge[d]	Hydrophobicity, H[e]	Hydrophobic moment, μ_H[e]
Crotalicidin (Ctn)	* * * * KRFKKFFKKVKKSVKKRLKKIFKKPMVIGVTIPF	4151.41 (4151.39)	98%	+16	0.263	0.440
Ctn [1-14]	KRFKKFFKKVKKSV	1797.30 (1797.31)	96%	+9	-0.012	0.763
Ctn [15-34]	KKRLKKIFKKPMVIGVTIPF	2371.10 (2371.11)	98%	+8	0.455	0.311

[a]Asterisk (*) indicates elastase putative cleavage sites (http://web.expasy.org/peptide_cutter/). Peptides are C-terminal amides. [b]Determined by LC−MS. Theoretical mass, in parentheses, from http://www.innovagen.se/custom-peptide-synthesis/peptide-property-calculator/peptide-property-calculator.asp). [c]By analytical HPLC, see Figure S1. [d]At neutral pH, from http://www.innovagen.se/custom-peptide-synthesis/peptide-property-calculator/peptide-property-calculator.asp). [e]From http://heliquest.ipmc.cnrs.fr/.

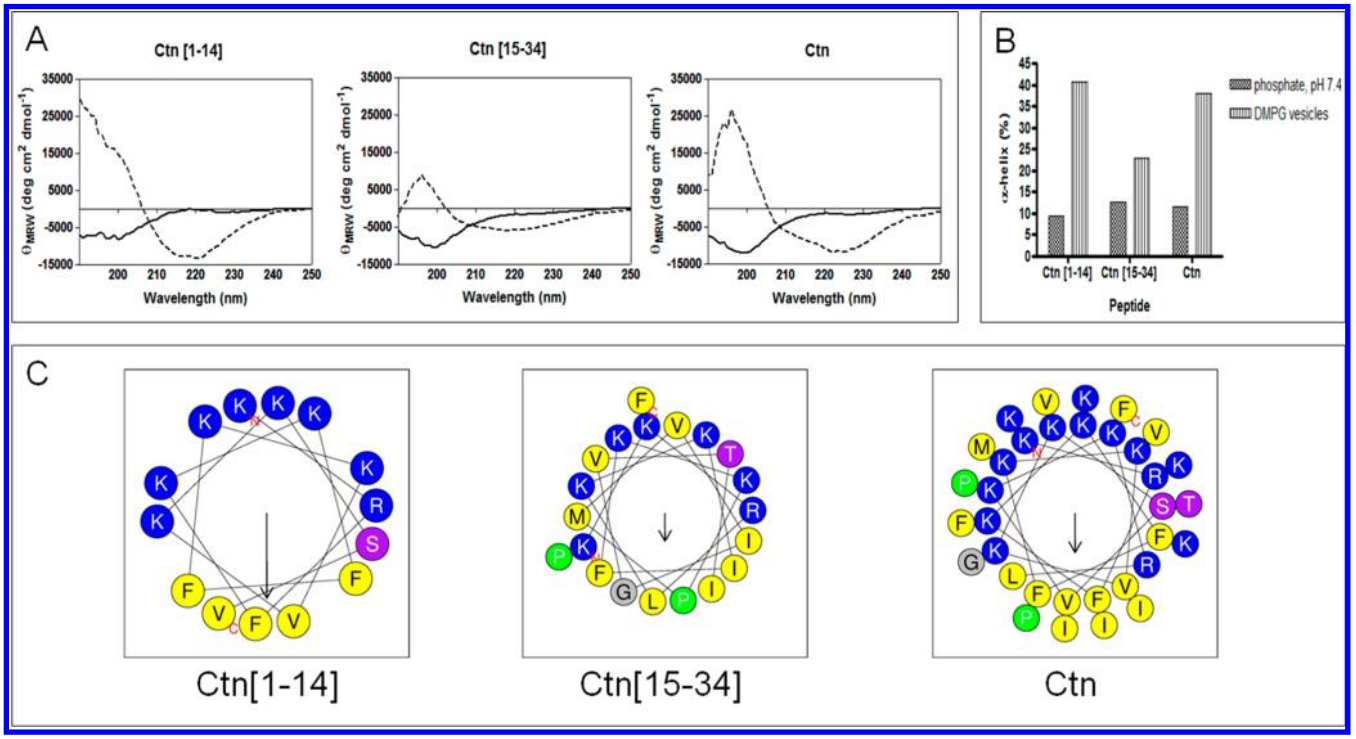

Figure 1. (A) CD spectra of Ctn and its Ctn[1−14] and Ctn[15−34] fragments in aqueous buffer (solid lines) and in contact with DMPG vesicles (dashed lines). (B) Percentage α-helix of each peptide alone in aqueous buffer or with DMPG vesicles. (C) Helical-wheel projections of each peptide.

CRAMPs (termed vipericidins), deduced by analysis of cDNA libraries from venom glands, were synthesized and tested against a panel of bacterial species and shown to have preferential activity against Gram-negative species.

Structure-guided dissection is a fruitful approach to define the minimally active regions of bioactive peptides.[19−22] Thus, for cathelicidins such as human LL-37, several fragments have been made and tested to define the minimal amphipathic α-helix structure(s) that could maintain or improve the antimicrobial activity of the parent peptide.[23−25] Herein we describe the dissection of crotalicidin (Ctn), one of the above-mentioned reptilian CRAMPs, into two segments with distinct structural features and biological activities. The boundary between the two segments was defined by bioinformatics prediction using elastase as a model for Ctn proteolysis. From a therapeutic standpoint, the 20-residue C-terminal segment, Ctn[15−34], turns out to be the most interesting one in that it replicates both the antimicrobial and antitumor profiles of the parent Ctn, yet it is less toxic to nontumor cells. Intriguingly, NMR analysis of Ctn[15−34] in a membrane-like environment shows it to be structurally unordered, while highly helical, amphipathic Ctn[1−14] is biologically unremarkable, hence challenging the accepted view that AMPs usually exert their action through the adoption of helical structures.

RESULTS

Structural Dissection of Ctn, Ctn[1−14], and Ctn[15−34] Fragments. The mature Ctn sequence (Table 1) was submitted to in silico proteolysis (http://web.expasy.org/peptide_cutter/) with elastase from neutrophils, which cuts at the carboxyl side of Val residues.[26] Out of four possible sites, cleavage at Val14 (Table 1) gave two fragments of similar length, Ctn[1−14] and Ctn[15−34], that were selected along with Ctn for this study. Interestingly, while this cleavage generated a similar distribution of basic (Lys, Arg) residues on each fragment (net charges of +9 and +8 for Ctn[1−14] and Ctn[15−34] at physiological pH, respectively), it produced a marked contrast in the hydrophobicities of both peptides (Table 1).

Synthetic replicas of Ctn[1−14] and Ctn[15−34] were prepared in C-terminal amide form by solid phase methods, as described for full-length Ctn.[18] The HPLC-purified peptides

DOI: 10.1021/acs.jmedchem.5b01142
J. Med. Chem. 2015, 58, 8553−8563

(Figure S1, Supporting Information) were satisfactorily characterized for purity by HPLC (all three peptides above 95% pure; see Table 1 and Supporting Information, Figure S1) and identity by electrospray MS (Table 1). 1 mM stock solutions of all three peptides were prepared in deionized water and stored for up to 6 weeks at 4 °C without any detectable degradation.

Circular Dichroism. The solution secondary structures of Ctn and its Ctn[1−14] and Ctn[15−34] fragments were first investigated by CD. In aqueous buffer, all three peptides displayed spectra (Figure 1A, solid lines) with a 200 nm negative band, typical of aperiodic conformation. In the presence of anionic lipid vesicles, the negative bands shifted to ∼220 nm (dashed lines), suggesting adoption of α-helical structure. The α-helix shift was more pronounced for Ctn and Ctn[1−14] (26% and 31% increase, respectively; Figure 1B) than for less environment-sensitive Ctn[15−34] (10% increase). Helical wheel plots (Figure 1C) show near-ideal amphipathic structure for Ctn[1−14], consistent with its high calculated hydrophobic moment of 0.763 (Table 1), while for Ctn ($\langle\mu_H\rangle$ = 0.440) and Ctn[15−34] ($\langle\mu_H\rangle$ = 0.311) the amphipathic distributions were far less perfect.

NMR Structures of Ctn and Derived Peptides in DPC Micelles. The structures of Ctn and its Ctn[1−14] and Ctn[15−34] fragments were next investigated by NMR spectroscopy in a membrane-like (DPC micelle) environment. Spectra were acquired at pH 3, which is more suitable than pH 7.0−7.5 for observing NH resonances. As the peptides do not contain any residues titrating in the pH 2−9 range (Asp, Glu, His), the pH change is unlikely to alter structural behavior. Since the spectra of Ctn and Ctn[15−34], each with two Pro residues in its sequence (Table 1), showed signals attributable to minor species resulting from Pro *cis*−*trans* isomerism, the rotameric state of Pro25 and Pro33 in the major species of both Ctn and Ctn[15−34] was first examined. The *trans* conformation of both Pro residues in each peptide was readily confirmed by the small difference in chemical shift between the $^{13}C_\beta$ and $^{13}C\gamma$ of the two Pro residues ($\Delta\delta^{Pro} = \delta_{C\beta} - \delta_{C\gamma}$; 4.2 and 3.9 ppm for Pro25 and Pro33 of Ctn; 4.6 and 4.1 ppm for Ctn[15−34], respectively, and 35 °C),[27] and by the characteristic sequential NOEs between the $\delta\delta'$ protons of Pro25 and Pro33 and the Hα protons of Pro-preceding residues, Lys24 and Ile32, respectively. Since very few signals attributable to the three possible minor rotamers (one with Pro25 in *cis* and Pro33 in *trans*; one with Pro25 in *trans* and Pro33 in *cis*; one with both Pro25 and Pro33 in *cis*) were detectable in the NMR spectra, these were not assigned. Hereafter, we refer only to NMR parameters of the major species.

After ^{1}H and ^{13}C chemical shift assignment (see Experimental Section), the first hints about the structural behavior of the three peptides came from the well-established empirical relationship between conformational shifts ($\Delta\delta = \delta^{observed} - \delta^{random\ coil}$, ppm) of both H_α protons and C_α carbons and dihedral ϕ and ψ angles. For full-length Ctn, plots of $\Delta\delta_{H\alpha}$ and $\Delta\delta_{C\alpha}$ vs sequence (Figure 2) exhibited two clearly distinct regions: a long stretch of negative $\Delta\delta_{H\alpha}$ and positive $\Delta\delta_{C\alpha}$ values spanning residues 3−21, and a shorter C-terminal segment with either null or very small ($\Delta\delta_{H\alpha}$ < 0.05 ppm and $\Delta\delta_{C\alpha}$ > 0.5 ppm) values except for Val30 and, as expected, the two Pro-preceding residues (Lys24 and Ile32). This profile suggested that the N-terminal region of Ctn was adopting a helical structure, whereas the C-terminal region was largely disordered, with perhaps some local nonrandom conformation

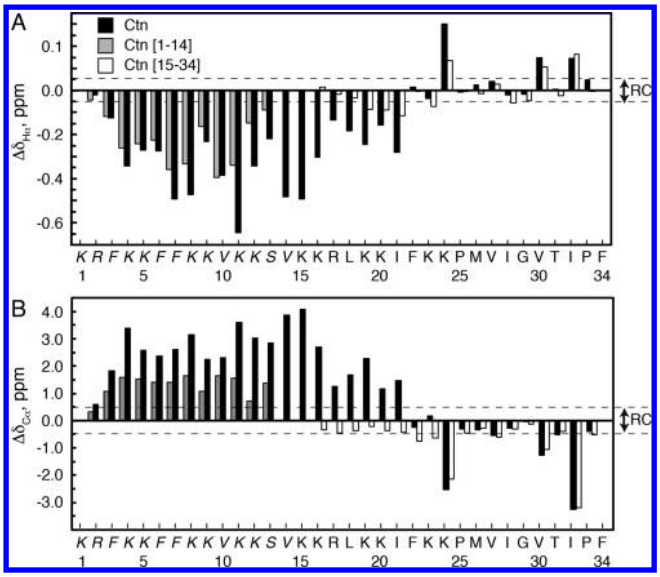

Figure 2. (A) $\Delta\delta_{H\alpha}$ ($\Delta\delta_{H\alpha} = \delta_{H\alpha}^{observed} - \delta_{H\alpha}^{RC}$, ppm) and (B) $\Delta\delta_{C\alpha}$ ($\Delta\delta_{C\alpha} = \delta_{C\alpha}^{observed} - \delta_{C\alpha}^{RC}$, ppm) values plotted as a function of sequence for Ctn (black bars), Ctn[1−14] (gray bars), and Ctn[15−34] (white bars) in 30 mM DPC-d38 at pH 3.0 and 25 °C. Ctn[1−14] residues are in italics. Values for N- and C-terminal residues are not shown. Random coil (RC) values were taken from Wishart et al.[58] Dashed lines indicate RC ranges.

around Val30. Further support for this conclusion came from the set of helix-characteristic NOEs observed for the 3−22 segment, i.e., intense sequential HN-HN and medium range αN(i,i+3) and $\alpha\beta$(i,i+3) (Figure 3). In contrast, only a few nonsequential NOEs were observed for residues 23−34.

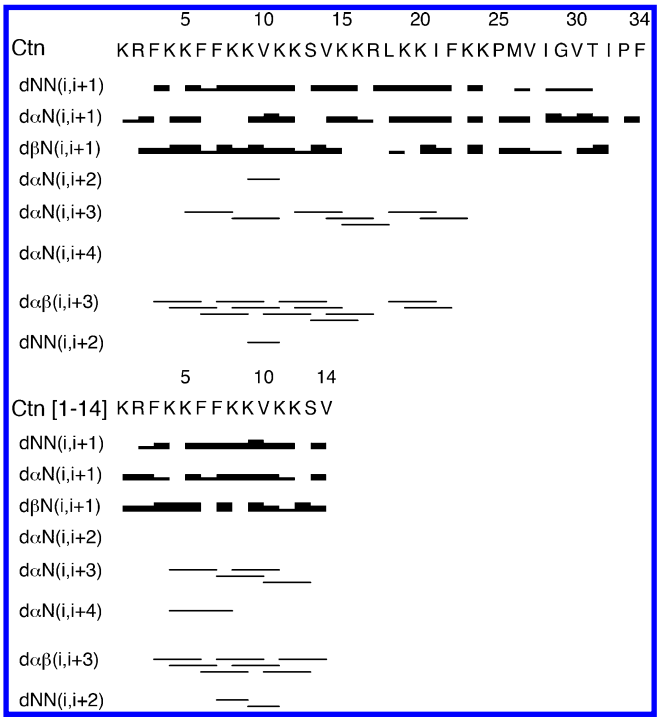

Figure 3. Summary of NOEs for Ctn and Ctn[1−14]. Intensities of sequential NOEs classified as strong, medium, and weak are indicated by the thickness of the lines.

DOI: 10.1021/acs.jmedchem.5b01142
J. Med. Chem. 2015, 58, 8553−8563

Table 2. Estimated Helix Populations in 30 mM DPC at pH 3 and 25°C and Relevant Structure Calculation Data for Peptides Ctn, Ctn[1−14], and Ctn[15−34]

	Ctn	Ctn[1−14]	Ctn[15−34]
helix length	3−21	3−13	16−21
averaged $\Delta\delta_{H\alpha}$, ppm	−0.32	−0.22	−0.07
% helix	82	57	17
no. of distance restraints	461	200	24
no. of dihedral angle constraints (ϕ, ψ)	59	24	29
pairwise rmsd (Å)			
backbone atoms[a]	0.5 ± 0.2 (3-21)	0.5 ± 0.2 (3−13)	0.5 ± 0.6 (17−21)
	2.5 ± 0.9 (23−33)		2.4 ± 0.9 (23−33)
all heavy atoms[a]	1.2 ± 0.2 (3−21)	1.7 ± 0.3 (3−13)	2.0 ± 0.7 (3−21)
	4 ± 1 (23−33)		3 ± 1 (23−33)

[a]Residues taken into consideration to calculate rmsd are indicated between parentheses.

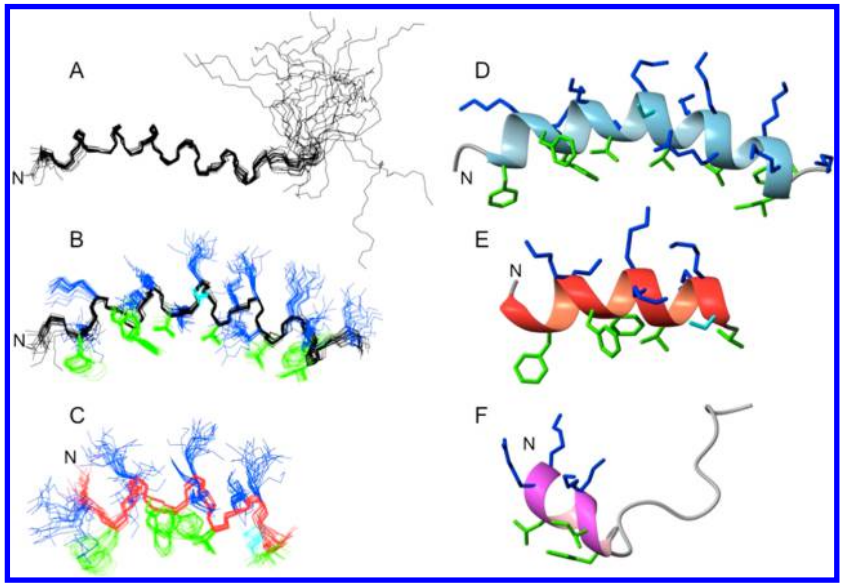

Figure 4. Ctn structures in DPC micelles. Representations of the 20 lowest target function calculated structures for (A) all backbone atoms of Ctn superposed over residues 3-21; (B) the N-terminal region, residues 1−21, of Ctn showing backbone atoms in black and side chains in blue if positively charged, in green if hydrophobic, and in cyan if polar; and (C) Ctn[1−14] showing backbone atoms in red and side chains colored as in panel B. Ribbon representations for the lowest target function structures of (D) Ctn, (E) Ctn[1−14], and (F) Ctn[15−34]. Side chains are in neon and colored as in panel B. In all the panels, an "N" labels the N terminus.

The $\Delta\delta_{H\alpha}$ and $\Delta\delta_{C\alpha}$ profiles and NOEs for Ctn[1−14] (Figures 2 and 3) were quite similar to the corresponding segments in Ctn, the main difference being the smaller magnitudes of $\Delta\delta_{H\alpha}$ and $\Delta\delta_{C\alpha}$ values relative to Ctn (Figure 2). From this it was concluded that Ctn[1−14] formed a helical structure, though less populated than in the full-length peptide. On the basis of the averaged $\Delta\delta_{H\alpha}$ values,[28,29] the helix populations of Ctn (residues 3-21) and Ctn[1−14] (residues 3−13) in DPC micelles at 25 °C, pH 3.0, were estimated as 82% and 57%, respectively (Table 2).

For Ctn[15−34], $\Delta\delta_{H\alpha}$ and $\Delta\delta_{C\alpha}$ values were mostly within the random coil range (Figure 2), with only a few nonsequential NOEs involving the side chains of Phe22 and Phe34 (Table S1, Supporting Information) and rather small negative $\Delta\delta_{H\alpha}$ values for residues 18−21 suggestive of a low populated helix (estimated as 17%, at 25 °C, Table 2).

To better visualize the 3D features of the peptides, structure calculations were performed (see Experimental Section and Table S1, Supporting Information). For Ctn, the structural ensemble was poorly defined (rmsd = 4.8 ± 1.8 Å for backbone atoms) if all residues were taken into account. However, on the basis of the above chemical shift and NOE data, it was possible to outline a well-defined N-terminal α-helix spanning residues 3−21 (Figure 4A, rmsd = 0.5 ± 0.2 Å for backbone atoms; Table S1) and a poorly structured C-terminal part (Figure S3, Supporting Info; rmsd = 2.5 ± 1.9 Å for backbone atoms of residues 23−33). Side chains of the α-helix were ordered (χ_1 variability of less than ±30°) and distributed as a rather amphipathic helix (Figure 4, panels B and D). For Ctn[1−14], the structural ensemble was a well-defined, amphipathic α-helix spanning residues 3−13 (Figure 4, panels C and E; rmsd = 0.6 ± 0.3 Å for backbone atoms of residues 2−13; Table 2), very similar to that of full-length Ctn (rmsd for backbone atoms of residues 3−13, Ctn[1−14] vs Ctn is 0.4 Å; Figure S4, Supporting Information).

For Ctn[15−34], as expected from the small number of observed nonsequential NOEs, the calculated structure was poorly defined, with a short amphipathic helix at the N-terminal end (Figure 4F) and some minor local structure around Pro33, with the side chains of Ile32 and Phe34 in close proximity (Figure S5, Supporting Information), a situation reminiscent of

DOI: 10.1021/acs.jmedchem.5b01142
J. Med. Chem. 2015, 58, 8553−8563

Table 3. Minimal Inhibitory Concentration (MIC) of Ctn and Fragments Ctn[1−14] and Ctn[15−34] against Standard and Clinical Strains of Different Bacterial Species[a]

		MIC, μM (μg/mL)			
microorganism	Gram	Ctn[1−14]	Ctn[15−34]	Ctn	gentamicin
E. faecalis (ATCC 29212)	+	71 (>128)	54 (>128)	7.7 (32)	17 (8)
E. faecalis (CI)	+	71 (>128)	54 (>128)	31 (128)	34 (16)
S. aureus (ATCC 29213)	+	71 (>128)	54 (>128)	7.7 (32)	0.5 (0.25)
S. aureus (CI)	+	71 (>128)	54 (>128)	7.7 (32)	0.5 (0.25)
S. pyogenes (CI)	+	36 (64)	3.4 (8)	3.8 (16)	17 (8)
P. aeruginosa (ATCC 27853)	−	71 (>128)	27 (64)	0.24 (1)	2.1 (1)
P. aeruginosa (CI)	−	71 (>128)	27 (64)	3.8 (16)	17 (8)
K. pneumoniae (CI)	−	71 (>128)	3.4 (8)	1.9 (8)	4.2 (2)
E. coli (ATCC 25922)	−	71 (>128)	0.11 (0.25)	0.06 (0.25)	1 (0.5)
E. coli (CI)	−	71 (>128)	3.4 (8)	3.8 (16)	34 (16)
A. baumannii (CI)	−	71 (>128)	1.7 (4)	3.8 (16)	17 (8)

[a]CI = clinical isolate.

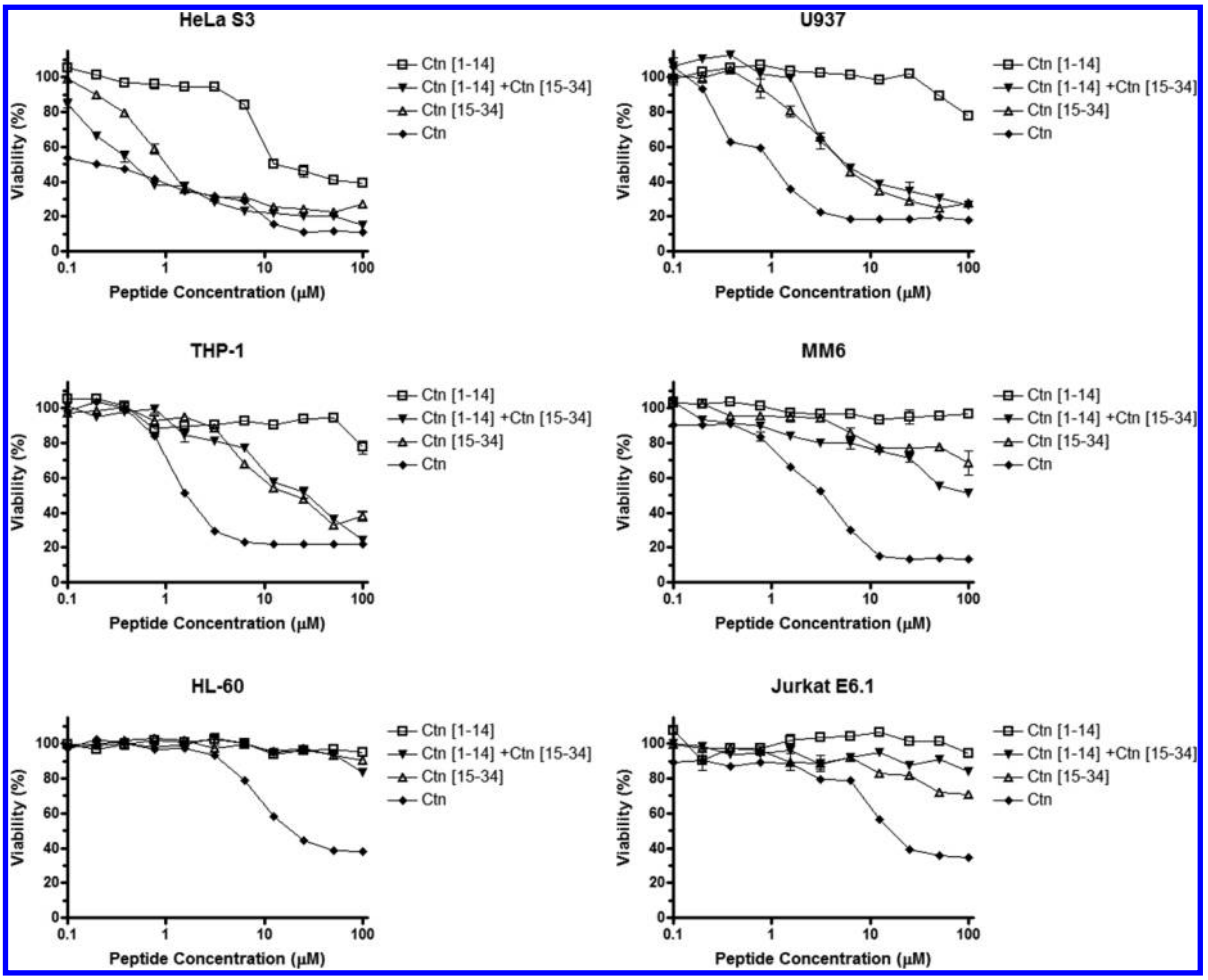

Figure 5. Viability of HeLa and leukemia cells upon treatment with Ctn and fragments for 4 h.

the corresponding region in full-length Ctn albeit with some variability among the structural ensembles.

Antimicrobial Activity. Given the good antimicrobial profile already reported for Ctn,[18] we decided to investigate to what extent it was preserved in the Ctn[1−14] and Ctn[15−34] peptides representing the N-terminal (α-helical) and the C-terminal (unstructured) segments. Table 3 summarizes the activity of Ctn, Ctn[1−14], and Ctn[15−34] against a panel of Gram-positive and -negative bacteria. As observed earlier,[18] Ctn is an effective antimicrobial, particularly against Gram-negatives, with MICs in the low μM range, often better than the gentamicin control, against both standard and clinical strains of *Pseudomonas aeruginosa*, *Klebsiella pneumoniae*, *Escherichia coli*, and *Acinetobacter baumannii*. Ctn[1−14], for its part, did not show any antimicrobial activity. On the other hand, Ctn[15−34], despite >40% size reduction relative to Ctn, showed an antimicrobial profile only slightly inferior than the parent peptide, again better in molar terms than gentamicin against *S.*

DOI: 10.1021/acs.jmedchem.5b01142
J. Med. Chem. 2015, 58, 8553−8563

pyogenes and three of the Gram-negatives, *K. pneumoniae, E. coli,* and *A. baumannii.*

Antitumor Activity. A next step was to investigate whether the activity of Ctn and its two fragments against bacteria was paralleled against tumor cells. For these experiments, the leukemia cell lines U937, THP-1, MM6, HL-60, and Jurkat E6.1 as well as HeLa S3 were used, and in addition to the three peptides an equimolar mixture of Ctn[1−14] and Ctn[15−34] was also tested to verify if noncovalent association of both peptides could be as effective as the parental compound. Cell viabilities were determined by measuring the decrease in metabolic activity with the nonfluorescent dye resazurin, which is reduced to fluorescent resorufin by live viable cells only. As shown in Figure 5, the peptides displayed selective toxicity in a concentration-dependent manner. Ctn was again the most toxic peptide, with IC_{50} values below 1 μM for HeLa S3 and U937, in the low μM range for THP-1 ($IC_{50} \approx 1.56$ μM) and MM6 ($IC_{50} \approx 3.12$ μM), and above 12.5 μM for HL-60 and Jurkat E6.1. As with bacteria, both Ctn[1−14] and Ctn[15−34] had differing behaviors toward tumor cells. While Ctn[15−34] was toxic for the most Ctn-sensitive cells (IC_{50} values of 1, 6.25, and 25 μM for HeLa S3, U937, and THP-1, respectively), Ctn[1−14] was toxic to HeLa S3 cells only above 10 μM and had practically no effects on leukemia cells. For the equimolar Ctn[1−14] + Ctn[15−34] mixture, practically no change in activity against most tumor cells was observed except for HeLa S3 and MM6 where a slight enhancement over that achieved with Ctn[15−34] alone was noted, albeit never reaching that of full-length Ctn. After 24 h of incubation, peptide toxicity against all tumor cell lines exhibited similar profiles to those at 4 h (compare Figure 5 and Figure S5, Supporting Information), although at the highest concentrations and longest incubation times a further decrease in viabilities could be observed, as expected.

Toxicity to Eukaryotic Cells. The toxicity of Ctn and its fragments Ctn[1−14] and Ctn[15−34] toward human fibroblasts and human erythrocytes, as representative healthy eukaryotic cells, was next investigated. Fibroblasts (1BR3G line) were submitted to the same metabolic assay in the same concentration range as tumor cells above. Figure 6 (top) shows that, as for tumor cells, Ctn was again the most toxic peptide, with $IC_{50} \approx 6.25$ μM after 4 h of incubation. Fragments Ctn[1−14] and Ctn [15−34] and their equimolar mixture had little toxicity toward fibroblasts, with only a 20% reduction in viability at 100 μM, the highest concentration tested. Toxicity profiles were similar after 24 h, though again only Ctn had noticeable effect on cell viability (Figure S6, Supporting Information).

The hemolytic effect of the peptides was tested on human erythrocytes and showed Ctn as a moderately lytic peptide (7% and 33% hemolysis at 100 and 400 μM, respectively), although far less than standard AMPs such as the cecropin A−melittin hybrid CA(1−8)M(1−18) (Figure 6, bottom). In contrast, Ctn[1−14] and Ctn[15−34] were totally nonhemolytic up to 400 μM, and their equimolar mixture at that concentration caused only 7% hemolysis.

Serum Stability. To further explore their therapeutic potential Ctn, Ctn[1−14], and Ctn[15−34] were tested for stability against human serum by LC−MS. For Ctn[1−14], relatively fast breakdown was observed (Figure 7), with 100% clearance after 6 h ($t_{1/2}$ = 21 min). Most cleavage products reflected trypsin-like cleavage, consistent with the presence of 7 Lys + 1 Arg residues; representative HPLC traces are shown in

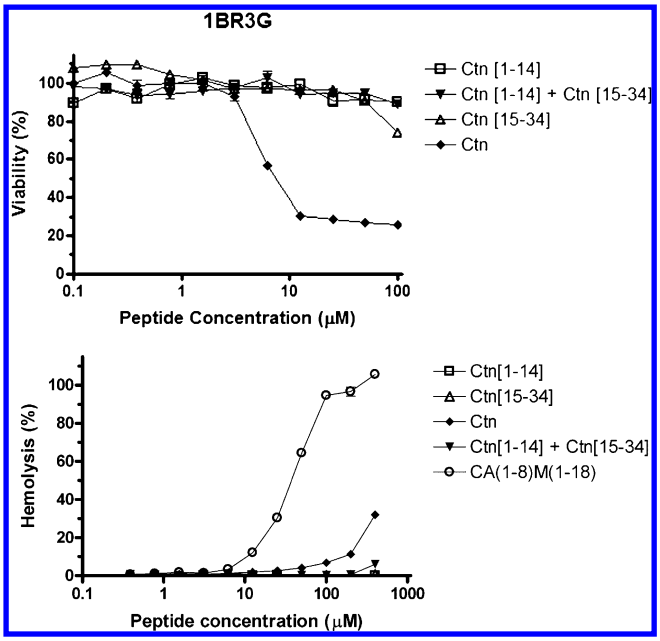

Figure 6. Toxicity of Ctn and fragments to eukaryotic cells: (top) 1BR3G fibroblast viability after 4 h; (bottom) hemolysis data.

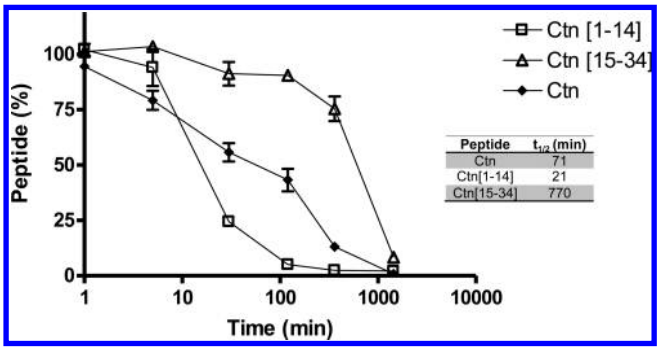

Figure 7. Time-course of the treatment of Ctn, Ctn[1−14], and Ctn[15−34] with human serum and (inset table) the corresponding half-lives.

Figures S7−S9, Supporting Information. Predictably, the protease lability of the N-terminal also caused a rather short lifetime for the full-length sequence, with $t_{1/2}$ = 71 min. In contrast, Ctn[15−34] proved remarkably resilient to serum degradation, with ∼10% peptide still remaining after 24 h incubation ($t_{1/2}$ = 770 min) (Figure 7).

DISCUSSION

In the unrelenting search for new medicines that can curb fast-spreading antibiotic resistance, AMPs have for some time been regarded as a promising alternative.[4,6,30,31] Until now, however, few AMPs have reached clinical trials and their use is mainly confined to topical applications. Despite some recognized advantages, clinical development of AMPs as anti-infectives is still hampered by issues such as low protease stability, potential toxicity, and high manufacturing costs. Protease susceptibility, with ensuing poor bioavailability, is particularly challenging and has been only partially addressed by strategies such as N- or C-terminal alteration (acetylation or amidation), site-specific changes (D- or artificial amino acid residues, peptidomimetics), prodrug approaches,[30,31] or encapsulation, which can also decrease toxicity.[32] However, as with other sequence-depend-

DOI: 10.1021/acs.jmedchem.5b01142
J. Med. Chem. 2015, 58, 8553−8563

ent properties, protease susceptibility or toxicity can be predicted only incompletely by bioinformatic approaches[33,34] and experimental validation is mandatory.

To address these toxicity and protease stability issues often preventing AMPs from advancing in the drug pipeline, we have performed a structural dissection of Ctn that has led to Ctn[15−34], a substantially (60%) downsized analogue with potential therapeutic application. Earlier work had already unveiled a potent antibacterial activity in Ctn,[18] but peptide size, at 34 residues, was a drawback, hence minimally active substructures were searched for. Similar structure-guided approaches with human cathelicidin LL-37 managed to downsize the parent molecule to fragments retaining amphipathic α-helical structure with the same or improved antimicrobial activity.[23−25] Also, Asian elapid CRAMPs have been modified in their α-helical domains to enhance antibiotic properties by the addition or removal of basic and/or hydrophobic residues.[35−37] In the present case, the known conversion of LL-37 by sweat proteases into fragments retaining the activity of the parent molecule[11] prompted us to simulate Ctn cleavage using neutrophil elastase as a model enzyme. For a snake venom peptide such as Ctn, the choice of elastase was justified in that neutrophils are present and release protease-containing granules at inflammation sites such as those in a bitten prey.[38] The in silico dissection at four possible cleavage sites generated eight pairwise fragments of which only the largest pair, Ctn[1−14] and Ctn[15−34], resulting from cleavage at Val14, was considered worth evaluating along with Ctn. All three peptides were synthesized as C-terminal carboxamides, a modification that entails a modest enhancement in proteolytic stability and has been previously applied to a fragment of LL-37[39] as well as to other AMPs.[40,41]

CD examination of the secondary structure of the three peptides in anionic DMPG micelles that resemble bacterial cell membranes showed a strong α-helical tendency for Ctn[1−14], also observed for the entire Ctn sequence, and a more disorganized structure, with lower helix propensity, for Ctn[15−34]. NMR experiments in the presence of DPC micelles simulating the neutral zwitterionic membranes of healthy eukaryotic cells corroborated CD results, revealing two distinct structural regions in Ctn (a well-defined helix at residues 3−21 followed by a rather unstructured C-terminal part) roughly around the putative elastase cleavage site.

Antimicrobial screening of Ctn and its fragments against a representative panel of Gram-positive and -negative organisms showed that the earlier reported strong bactericidal activity of the full-length peptide[18] is largely confined to the C-terminal Ctn[15−34] section, while the N-terminus, regardless of its strong cationic (8 basic residues out of 14) and amphipathic α-helical nature (predictable from the calculated μ_H = 0.763 (Table 1), the highest of all three peptides and experimentally confirmed by NMR (Figure 4C and Figure 4E)), was devoid of significant AMP properties. This lack of activity of a strongly cationic, amphipathic helical peptide such as Ctn[1−14] is somewhat puzzling, at least in terms of the conventional paradigm whereby AMP action is associated with amphipathic α-helical structures rich in basic (Lys, Arg) residues (e.g., cecropins, magainins, melittin). Thus, when the Ctn sequence is run on an AMP prediction algorithm,[42] the 22-residue segment from the N-terminus, comprising Ctn[1−14], is (inaccurately) predicted as antimicrobial.

As a possible explanation for such noncompliance of Ctn[1−14] with the predictions, it might be argued that the high μ_H value[43] calculated for the N-terminal segment does not realistically estimate its AMP potential, since its low content in hydrophobic residues (only 1/3 of total, H = −0.012, Table 1) may affect its global ability to interact with lipid bilayers. Indeed, the simplistic view of cationic, amphipathic α-helices as mandatory for AMP action has been convincingly challenged[44,45] by showing that AMPs lacking α-helical structure but with amphipathic features (i.e., diastereomers of canonical AMPs made by educated D-amino acid replacements) can be designed as effective antimicrobials; hence, amphipathicity though not α-helicity appears to be the requirement. In any event, our data on cationic, α-helical, amphipathic yet inactive Ctn[1−14], as well as on poorly structured but active Ctn[15−34] (see below), constitute a salutary reminder that even the best structure-based predictions of AMP activity are no substitute for experimental validation.

While for Gram-positive bacteria except *S. pyogenes* (Table 3), Ctn[15−34] significantly underperformed Ctn; for Gram-negatives it matched to a reasonable extent the antimicrobial behavior of the parental structure, despite the substantial size reduction (42%) relative to Ctn and the low helicity and nonideal amphipathicity revealed by CD and NMR. Of note are the low-μM MICs of Ctn[15−34] against clinical isolates of *K. pneumoniae* and, particularly, *E. coli* and *A. baumannii*, which outdid a reference antibiotic such as gentamicin by about 1 order of magnitude on a molar basis. Hence, it seems that preserving one-half of the positive charge of Ctn but substantially increasing hydrophobicity (0.455 vs 0.263, Table 1) turns Ctn[15−34] into a peptide that, while less amphipathic than the parent Ctn, can effectively target the anionic membranes and/or the lipopolysaccharide of Gram-negative bacteria although it loses all activity toward Gram-positives. Interestingly, the rather equivalent antimicrobial profiles of Ctn and Ctn[15−34] against Gram-negatives (except *P. aeruginosa*) did not apply to eukaryotic cells such as fibroblasts or erythrocytes, for both of which the full-length peptide proved to be rather toxic whereas Ctn[15−34] was practically innocuous. It would appear that the size reduction in Ctn[15−34], plus the loss of half the positive charges and the increase in hydrophobicity relative to Ctn, caused weaker interactions with the membranes of healthy eukaryotic cells, composed mainly of zwitterionic phospholipids and cholesterol.

As antitumor activity is often observed alongside microbicidal properties in many AMPs,[7,8] the three peptides of this study were accordingly tested against various tumor cell lines (Figure 5). In tune with the above-mentioned toxicity to healthy eukaryotic cells, Ctn was also rather cytotoxic against both HeLa and leukemia cells, whereas Ctn[1−14] and Ctn[15−34] were, respectively, practically ineffective (active only against HeLa at >10 μM) and active on those cell types most susceptible to Ctn, i.e., HeLa S3, U937, and THP-1, with IC_{50} values not widely different from those of the parent peptide. The toxicity of Ctn[15−34] toward cancer cells did not significantly improve by admixture with Ctn[1−14], strongly suggesting that the bioactive structure (hence maximal antitumor activity) is achieved only by the full Ctn sequence, not by a combined effect of its fragments.

Taken together, the evidence collected thus far (bacterial MICs, antitumor activity, toxicity to nontumor cells) portrays Ctn as a toxic peptide with a rather indiscriminate killing effect on bacteria, tumor, and nontumor cells, hence with limited therapeutic potential. The N-terminal Ctn[1−14] segment, for its part, has lost practically all the antimicrobial and antitumor

DOI: 10.1021/acs.jmedchem.5b01142
J. Med. Chem. 2015, 58, 8553−8563

activity of the parental sequence and thus lacks interest for either anti-infective or antitumor applications. In contrast, Ctn[15−34] preserves most of the antimicrobial activity of Ctn, particularly against Gram-negatives, and its slightly inferior cytotoxicity to tumor cells relative to Ctn is more than made up by its practically nil toxicity toward healthy eukaryotic cells (Figure 6). All these features plus a more convenient size (20 vs 34 residues), hence ease of production, and, last but not least, a definitely remarkable stability in human serum (Figure 7) combine to make Ctn[15−34] a rather promising peptide lead for potential development into an anti-infective or (more likely) an antitumor agent.

EXPERIMENTAL SECTION

Bioinformatic Analyses. The Ctn sequence[18] was run on the "Peptide Cutter" (http://web.expasy.org/peptide_cutter/) software with neutrophil elastase as model protease. Ctn and its Ctn[1−14] and Ctn[15−34] fragments were also run on the "Peptide property calculator" (http://www.innovagen.se/custom-peptide-synthesis/peptide-property-calculator/peptide-property-calculator.asp) and "Heliquest"[46] (http://heliquest.ipmc.cnrs.fr/) software to determine molecular weight, net charge, hydrophobicity, and hydrophobic moment data in Table 1, as well as the helical-wheel plots in Figure 1.

Peptide Synthesis. Ctn, Ctn[1−14], and Ctn[15−34] were synthesized in C-terminal carboxamide form in an ABI433 instrument (Applied Biosystems, Foster City, CA) running Fmoc (FastMoc) SPPS protocols at 0.1 mmol scale on a Fmoc-Rink-amide ChemMatrix resin. Side chain functionalities were protected with *tert*-butyl (Glu, Ser, Thr, Tyr), N^G-2,2,4,6,7-pentamethyldihydrobenzofuran-5-sulfonyl (Arg), and trityl (Cys) groups. Eight-fold excess of Fmoc-L-amino acids and HBTU, in the presence of a double molar amount of DIEA, were used for the coupling steps, with DMF as solvent. After chain assembly, full deprotection and cleavage were carried out with TFA/H_2O/TIS (95:2.5:2.5 v/v, 90 min, rt). Peptides were precipitated by addition of chilled diethyl ether, taken up in aqueous HOAc (0.1 M) and lyophilized. Analytical reversed-phase HPLC was performed on a Luna C18 column (4.6 mm × 50 mm, 3 μm; Phenomenex, Jupiter, CA). Linear gradients of solvent B (0.036% TFA in MeCN) into A (0.045% TFA in H_2O) were used for elution at a flow rate of 1 mL/min and with UV detection at 220 nm. Preparative HPLC runs were performed on a Luna C18 column (21.2 mm × 250 mm, 10 μm; Phenomenex, Jupiter, CA), using linear gradients of solvent B (0.1% in MeCN) into A (0.1% TFA in H_2O), as required, with a flow rate of 25 mL/min. Fractions of adequate HPLC homogeneity and with the expected mass were combined and lyophilized. LC−MS was performed in a LC−MS 2010EV instrument (Shimadzu) fitted with an XBridge C18 column (4.6 mm × 150 mm, 3.5 μm, Waters, Cerdanyola del Vallès, Spain), eluting with linear gradients of HCOOH/MeCN (0.08% v/v) into HCOOH/H_2O (0.1%, v/v) over 15 min at 1 mL/min. Peptide stock solutions (1 mM) in H_2O were stored at 4 °C, periodically checked for stability by LC−MS for up to 6 weeks, and made afresh as required.

Circular Dichroism. CD spectra of the peptides were acquired in a J-815 spectropolarimeter (Jasco, Tokyo, Japan) at 25 °C in the 190−250 nm wavelength range, with a bandwidth of 1 nm and a scan speed of 50 nm/min, using a 0.1 cm quartz cell. 70 μM peptide solutions were prepared in 10 mM sodium phosphate buffer (pH 7.4) in the absence or presence of 6 mM DMPG vesicles (Sigma-Aldrich, Madrid, Spain). Vesicles were prepared by dissolving dry DMPG in chloroform/methanol (2:1), removing the solvents under reduced pressure with a N_2 flow, and drying the resulting lipid films overnight in a freeze-dryer. The next day, lipid films were hydrated with 10 mM sodium phosphate, mixed in a vortex shaker, and sonicated until clear.

The final spectra for each peptide were the average of three consecutive scans per sample after subtraction of buffer and vesicle baselines. Results were expressed as mean residue ellipticity ($[\theta]_{MRW}$) (deg × cm^2 × $dmol^{-1}$), as follows:

$$[\theta]_{MRW} = \frac{(\theta_{obs} \times MRW)}{10dc}$$

where θ_{obs} is the observed ellipticity in degrees, MRW is the mean residue weight, d is the cell path length and c is the peptide molar concentration. The percentage of α-helix structure was estimated as

$$\%\ \alpha\text{-helix} = \frac{-[\theta]_{222nm} + 3000}{39000}$$

where $[\theta]_{222nm}$ is the mean residue ellipticity at 222 nm.[47,48]

NMR Spectroscopy. Samples were prepared by dissolving the lyophilized peptides (1−2 mg) in 0.5 mL of a fresh solution of 30 mM DPC-d38 (98% deuteration; Cambridge Isotope Laboratories, Tewksbury, MA) at pH 3.0 in either H_2O/D_2O (9:1 v/v) or pure D_2O. Peptide concentrations were approximately 1 mM. Sodium 2,2-dimethyl-2-silapentane-5-sulfonate was added as an internal reference. pH was measured with a glass microelectrode and not corrected for isotope effects and adjusted, if necessary, by adding minimal amounts of NaOD or DCl.

NMR spectra were recorded in a Bruker AV-600 spectrometer operating at a 600.13 MHz proton frequency and equipped with a cryoprobe. Probe temperature was calibrated using a methanol sample. 1D and 2D spectra, i.e., phase-sensitive correlated spectroscopy (COSY), total correlated spectroscopy (TOCSY), nuclear Overhauser enhancement spectroscopy (NOESY), and $^1H-^{13}C$ heteronuclear single quantum coherence spectra (HSQC), were acquired using standard pulse sequences and processed with the TOPSPIN program, as reported.[49] TOCSY and NOESY mixing times were 60 and 150 ms, respectively. $^1H-^{13}C$ HSQC spectra were acquired at natural heteronuclear abundance. The ^{13}C δ-values were indirectly referenced using the IUPAC-recommended $^{13}C/^1H$ ratio 0.251 449 53.[50]

^1H and ^{13}C assignment was achieved by standard sequential analysis[51,52] of 2D COSY, TOCSY, and NOESY spectra acquired at 25 and 35 °C, examined in combination with the corresponding 2D $^1H-^{13}C$ HSQC spectra. The ^{13}C chemical shift values served to confirm assignment of side chains, in particular the repeated Lys residues (13, 7, and 6 in Ctn, Ctn[1−14], and Ctn[15−34], respectively; Table 1). Chemical shifts for the three peptides have been deposited at the BioMagResBank (http://www.bmrb.wisc.edu) with accession codes 25363 (Ctn), 25366 (Ctn [1−14]), and 25370 (Ctn[15−34]).

NMR Structure Calculation. Structure calculations were performed with the CYANA 2.1 program.[53,54] Upper limit distance restraints were obtained from the NOE cross-peaks present in 2D NOESY spectra recorded at 25 and 35 °C, which were integrated using the automatic integration subroutine of the Sparky program (T. D. Goddard and D. G. Kneller, Sparky 3, NMR assignment program, University of California, San Francisco, USA). Restraints for the ϕ and ψ dihedral angles were derived from the $^1H_\alpha$, $^{13}C_\alpha$ and $^{13}C_\beta$ chemical shifts using the TALOS program.[55] For Ctn and Ctn[15−34], the standard iterative protocol for automatic NOE assignment implemented in CYANA 2.1[53] was used. It consists of seven cycles of combined NOE assignment and structure calculation of 100 conformers per cycle. The distance restraints resulting from the seventh cycle were checked by re-examination of the NOESY spectra, and if necessary, ambiguous constraints were removed or relaxed to generate the final list used as input for a standard CYANA2.1 simulated annealing calculation of 100 conformers. For each peptide, the final NMR structure corresponds to the ensemble of the 20 conformers with the lowest target function value. The Ctn structure has been deposited at the PDB Data Bank with accession code 2MWT. Statistics for the structural ensembles of the peptides are given in Table S1, Supporting Information.

As automatic NOE assignment is not applicable to mainly random peptides, the structure of Ctn[15−34] was calculated by a standard CYANA 2.1 protocol, using as distance restraints only the non-sequential ones (Tables S1 and S2, Supporting Information). In poorly structured peptides, random conformers contribute to the intensity of intraresidual and sequential NOEs. MOLMOL[56] was used to visualize the structures of the three peptides.

DOI: 10.1021/acs.jmedchem.5b01142
J. Med. Chem. 2015, 58, 8553−8563

Bacterial Strains and Antibacterial Assays. Assays were performed on reference strains of *E. coli* (ATCC 25922), *P. aeruginosa* (ATCC 27853), *E. faecalis* (ATCC 29212), and *S. aureus* (ATCC 29213). Clinical strains of *E. faecalis*, *S. aureus*, *E. coli*, *P. aeruginosa*, *K. pneumoniae*, *A. baumannii*, and *S. pyogenes* were also used. Isolates were thawed and transferred at least twice on sheep blood agar to ensure purity and good growth and incubated for 24 h prior to testing. Inocula were prepared by direct suspension of cells into saline to achieve the turbidity of the 0.5 McFarland standard. Minimal inhibitory concentration (MIC) assays were performed by the microdilution method in Mueller–Hinton broth according to Clinical and Laboratory Standards Institute (CLSI) guidelines.[57] For *S. pyogenes*, the MIC assay was performed in Mueller Hinton broth supplemented with lysed horse blood (5%). Gentamicin was used as control antibiotic.

Cell Culture. Human HeLa S3 (cervix epithelial carcinoma), leukemia Jurkat E6.1 (T-cell lineage), HL-60 (promyelocyte lineage), U937, THP-1, and MM6 (monocyte-macrophage lineage) cancer cells, and 1BR3G human fibroblasts were obtained from the Cell Line Repository of the Institut Municipal d'Investigaciò Mèdica (Barcelona, Spain). Cells were cultured in Dulbecco's modified Eagle medium (DMEM) supplemented with 10% fetal bovine serum (FBS) and 1% penicillin/streptomycin solution and maintained in T-25 cm^2 flasks at 37 °C in a humidified atmosphere with 5% CO_2. Cultures were maintained at 10^5–10^6 cell/mL densities. For 1BR3G fibroblasts, cells were split every time they reached 80–90% confluence after being harvested with PBS containing 0.025% (w/v) trypsin and 0.01% EDTA.

Peptide Cytotoxicity. About 60 000 cells were added to different microfuge tubes containing 2-fold serial dilutions of the peptides (final concentrations in the 0.1–100 μM range) in DMEM containing 2% FBS. After 30 min of incubation at 37 °C and 5% CO_2, 50 μL of medium containing approximately 10 000 treated cells were transferred to 96-well plates. Next, an amount of 15 μL of Cell Titer Blue dye (Promega, Madison, WI) was added to each well, and plates were reincubated for up to 24 h. Fluorescence at 4 and 24 h after dye addition was measured in an Infinite 200 (Tecan, Männedorf, Switzerland) reader, with λ_{exc} = 530 nm and λ_{em} = 590 nm. For 1BR3G fibroblasts, 5000 cells/well were seeded into 96-well plates. After 24 h of incubation at 37 °C and 5% CO_2, medium was removed and fresh medium containing 2% FBS and the various serial dilutions of the peptides was added. After 30 min of additional incubation, 15 μL of Cell Titer Blue was added to each well and readings were done as above. Relative cell viability was calculated with cells treated with only DMEM containing 2% FBS as controls (~100% viability). Assays were carried out in triplicate.

Hemolytic Activity. Fresh human blood (10 mL) was collected in EDTA tubes and centrifuged at 1000*g* for 10 min at 4 °C. After plasma removal, the pellet containing erythrocytes was washed three times with PBS and resuspended in PBS to obtain an 8% (v/v) suspension. 100 μL aliquots of erythrocyte suspension were added to microcentrifuge tubes, each containing 100 μL of 2-fold serially diluted peptide (0.2–800 μM) to final concentrations of 4% (v/v) and 0.1–400 μM, respectively. The suspensions were incubated for 30 min at 37 °C with gentle agitation, then centrifuged for 2 min at 1000*g*. Supernatants were transferred to 96-well plates, and hemoglobin release was measured by absorbance at 540 nm in an Infinite 200 (Tecan) multiplate reader. Triton X-100 at 1% and 4% (v/v) erythrocytes in PBS with no peptides (nontreated) were used as positive and negative controls, respectively. Percentage hemolysis was determined as $[(Abs_{540nm}$ peptide-treated $- Abs_{540nm}$ nontreated$)/(Abs_{540nm}$ 1% Triton X-100 $- Abs_{540nm}$ nontreated$)] \times 100$. Measurements were carried out in triplicate.

Serum Stability. Amounts of 0.5 mL each of human serum (Sigma) and peptide (1 mM in H_2O) were combined and incubated for 24 h at 37 °C with gentle swirling. 120 μL aliquots were taken at 0, 1, 5, 10, 30, 120, 360, and 1440 min, treated with 20 μL of trichloroacetic acid (15% v/v in H_2O) for 30 min at 4 °C, and centrifuged at 13 000 rpm for 10 min to remove serum proteins. The supernatant was analyzed by LC–MS in XBridge C18 or C8 columns (4.6 mm × 150 mm, 3.5 μm, Waters), eluting with linear gradients of HCOOH/MeCN (0.08% v/v) into HCOOH/H_2O (0.1%, v/v) over 15 min at 1 mL/min.

■ ASSOCIATED CONTENT

Supporting Information

The Supporting Information is available free of charge on the ACS Publications website at DOI: 10.1021/acs.jmedchem.5b01142.

Analytical data (HPLC traces) of the peptides; additional NMR data (NOESY spectra showing *i*, *i* + 3 NOEs, nonsequential NOEs in Ctn[15–34], structures of all three peptides); relative viabilities of tumor cells treated with peptides for 24 h; serum stability data (PDF)

■ AUTHOR INFORMATION

Corresponding Authors

*G.R.-B.: phone, +55-85999245081; e-mail, gandhi.radis@ufc.br.

*D.A.: phone, +34-933160868; fax, +34-933161901; e-mail, david.andreu@upf.edu.

Author Contributions

⊥C.B.F., C.P.-P., and B.G.d.l.T. contributed equally.

Notes

The authors declare no competing financial interest.

■ ACKNOWLEDGMENTS

Research at Federal University of Ceará was supported by the Brazilian National Council for Scientific and Technological Development (CNPq), by the Ministry of Science and Technology, and by the Coordination for the Improvement of Higher Education Personnel (CAPES). Research at Pompeu Fabra University was supported by the Spanish Ministry of Economy and Competitiveness (MINECO, Grant SAF 2011-24899) and by Generalitat de Catalunya (Grant SGR2009-00492). Research at the Instituto de Química Física Rocasolano (IQFR-CSIC) was supported by MINECO (Project CTQ2011-22514; Grant FPI BES-2012-057717 to H.Z.-C.). We thank Prof. Jordi Vila, Servei de Microbiologia, Hospital Clínic, Universitat de Barcelona, for antimicrobial assays. Mobility support from the European Commission, Marie Curie Actions, International Research Staff Exchange Scheme (No. 247513, MEMPEPACROSS), is gratefully acknowledged.

■ ABBREVIATIONS USED

AMP, antimicrobial peptide; COSY, correlation spectroscopy; DIEA, *N*,*N*-diisopropylethylamine; DMPG, 1,2-dimyristoyl-*sn*-glycero-3-phospho-*rac*-(1-glycerol); DPC-d38, [$^2H_{38}$]dodecylphosphocholine; HBTU, 2-(1*H*-benzotriazol-1-yl)-1,1,3,3-tetramethyluronium hexafluorophosphate; HSQC, heteronuclear single quantum coherence; MeCN, acetonitrile; MIC, minimum inhibitory concentration; NOE, nuclear Overhauser effect; NOESY, nuclear Overhauser effect spectroscopy; TFA, trifluoroacetic acid; TIS, triisopropylsilane; TOCSY, total correlation spectroscopy

■ REFERENCES

(1) *Antimicrobial Resistance: Global Report on Surveillance*; World Health Organization (WHO): Geneva, Switzerland, 2014; http://www.who.int (accessed Feb 11, 2015).

DOI: 10.1021/acs.jmedchem.5b01142
J. Med. Chem. 2015, 58, 8553–8563

(2) Brusselaers, N.; Vogelaers, D.; Blot, S. The rising problem of antimicrobial resistance in the intensive care unit. *Ann. Intensive Care* **2011**, *1*, 47.
(3) French, G. L. Clinical impact and relevance of antibiotic resistance. *Adv. Drug Delivery Rev.* **2005**, *57* (10), 1514−1527.
(4) Hadley, E. B.; Hancock, R. E. Strategies for the discovery and advancement of novel cationic antimicrobial peptides. *Curr. Top. Med. Chem.* **2010**, *10* (18), 1872−1881.
(5) Zaiou, M. Multifunctional antimicrobial peptides: therapeutic targets in several human diseases. *J. Mol. Med. (Heidelberg, Ger.)* **2007**, *85* (4), 317−329.
(6) Hancock, R. E.; Sahl, H. G. Antimicrobial and host-defense peptides as new anti-infective therapeutic strategies. *Nat. Biotechnol.* **2006**, *24* (12), 1551−1557.
(7) Gaspar, D.; Veiga, A. S.; Castanho, M. A. From antimicrobial to anticancer peptides. A review. *Front. Microbiol.* **2013**, *4*, 294.
(8) Schweizer, F. Cationic amphiphilic peptides with cancer-selective toxicity. *Eur. J. Pharmacol.* **2009**, *625* (1−3), 190−194.
(9) Zanetti, M. Cathelicidins, multifunctional peptides of the innate immunity. *J. Leukocyte Biol.* **2004**, *75* (1), 39−48.
(10) Bals, R.; Wilson, J. M. Cathelicidins–a family of multifunctional antimicrobial peptides. *Cell. Mol. Life Sci.* **2003**, *60* (4), 711−720.
(11) Murakami, M.; Lopez-Garcia, B.; Braff, M.; Dorschner, R. A.; Gallo, R. L. Postsecretory processing generates multiple cathelicidins for enhanced topical antimicrobial defense. *J. Immunol.* **2004**, *172* (5), 3070−3077.
(12) Chen, Y. P.; Chen, F. Identifying targets for drug discovery using bioinformatics. *Expert Opin. Ther. Targets* **2008**, *12* (4), 383−389.
(13) Wishart, D. S. Bioinformatics in drug development and assessment. *Drug Metab. Rev.* **2005**, *37* (2), 279−310.
(14) Zhao, H.; Gan, T. X.; Liu, X. D.; Jin, Y.; Lee, W. H.; Shen, J. H.; Zhang, Y. Identification and characterization of novel reptile cathelicidins from elapid snakes. *Peptides* **2008**, *29* (10), 1685−1691.
(15) Wang, Y.; Hong, J.; Liu, X.; Yang, H.; Liu, R.; Wu, J.; Wang, A.; Lin, D.; Lai, R. Snake cathelicidin from Bungarus fasciatus is a potent peptide antibiotics. *PLoS One* **2008**, *3* (9), e3217.
(16) Zhou, H.; Dou, J.; Wang, J.; Chen, L.; Wang, H.; Zhou, W.; Li, Y.; Zhou, C. The antibacterial activity of BF-30 in vitro and in infected burned rats is through interference with cytoplasmic membrane integrity. *Peptides* **2011**, *32* (6), 1131−1138.
(17) Wang, H.; Ke, M.; Tian, Y.; Wang, J.; Li, B.; Wang, Y.; Dou, J.; Zhou, C. BF-30 selectively inhibits melanoma cell proliferation via cytoplasmic membrane permeabilization and DNA-binding in vitro and in B16F10-bearing mice. *Eur. J. Pharmacol.* **2013**, *707* (1−3), 1−10.
(18) Falcao, C. B.; de La Torre, B. G.; Perez-Peinado, C.; Barron, A. E.; Andreu, D.; Radis-Baptista, G. Vipericidins: a novel family of cathelicidin-related peptides from the venom gland of South American pit vipers. *Amino Acids* **2014**, *46* (11), 2561−2571.
(19) Romestand, B.; Molina, F.; Richard, V.; Roch, P.; Granier, C. Key role of the loop connecting the two beta strands of mussel defensin in its antimicrobial activity. *Eur. J. Biochem.* **2003**, *270* (13), 2805−2813.
(20) Vila-Perello, M.; Tognon, S.; Sanchez-Vallet, A.; Garcia-Olmedo, F.; Molina, A.; Andreu, D. A minimalist design approach to antimicrobial agents based on a thionin template. *J. Med. Chem.* **2006**, *49* (2), 448−451.
(21) Radis-Baptista, G.; de la Torre, B. G.; Andreu, D. A novel cell-penetrating peptide sequence derived by structural minimization of a snake toxin exhibits preferential nucleolar localization. *J. Med. Chem.* **2008**, *51* (22), 7041−7044.
(22) Torrent, M.; Pulido, D.; de la Torre, B. G.; Garcia-Mayoral, M. F.; Nogues, M. V.; Bruix, M.; Andreu, D.; Boix, E. Refining the eosinophil cationic protein antibacterial pharmacophore by rational structure minimization. *J. Med. Chem.* **2011**, *54* (14), 5237−5244.
(23) Wang, G.; Mishra, B.; Epand, R. F.; Epand, R. M. High-quality 3D structures shine light on antibacterial, anti-biofilm and antiviral activities of human cathelicidin LL-37 and its fragments. *Biochim. Biophys. Acta, Biomembr.* **2014**, *1838* (9), 2160−2172.
(24) Dannehl, C.; Gutsmann, T.; Brezesinski, G. Surface activity and structures of two fragments of the human antimicrobial LL-37. *Colloids Surf., B* **2013**, *109*, 129−135.
(25) Nagant, C.; Pitts, B.; Nazmi, K.; Vandenbranden, M.; Bolscher, J. G.; Stewart, P. S.; Dehaye, J. P. Identification of peptides derived from the human antimicrobial peptide LL-37 active against biofilms formed by Pseudomonas aeruginosa using a library of truncated fragments. *Antimicrob. Agents Chemother.* **2012**, *56* (11), 5698−5708.
(26) Hedstrom, L. Serine protease mechanism and specificity. *Chem. Rev.* **2002**, *102* (12), 4501−4524.
(27) Schubert, M.; Labudde, D.; Oschkinat, H.; Schmieder, P. A software tool for the prediction of Xaa-Pro peptide bond conformations in proteins based on 13C chemical shift statistics. *J. Biomol. NMR* **2002**, *24* (2), 149−154.
(28) Vila, R.; Ponte, I.; Jimenez, M. A.; Rico, M.; Suau, P. A helix-turn motif in the C-terminal domain of histone H1. *Protein Sci.* **2000**, *9* (4), 627−636.
(29) Jimenez, M. A.; Barrachi-Saccilotto, A. C.; Valdivia, E.; Maqueda, M.; Rico, M. Design, NMR characterization and activity of a 21-residue peptide fragment of bacteriocin AS-48 containing its putative membrane interacting region. *J. Pept. Sci.* **2005**, *11* (1), 29−36.
(30) Hancock, R. E.; Sahl, H. G. New strategies and compounds for anti-infective treatment. *Curr. Opin. Microbiol.* **2013**, *16* (5), 519−521.
(31) Yeung, A. T.; Gellatly, S. L.; Hancock, R. E. Multifunctional cationic host defence peptides and their clinical applications. *Cell. Mol. Life Sci.* **2011**, *68* (13), 2161−2176.
(32) Torchilin, V. P. Recent advances with liposomes as pharmaceutical carriers. *Nat. Rev. Drug Discovery* **2005**, *4* (2), 145−160.
(33) Sharma, A.; Singla, D.; Rashid, M.; Raghava, G. P. Designing of peptides with desired half-life in intestine-like environment. *BMC Bioinf.* **2014**, *15*, 282.
(34) Gupta, S.; Kapoor, P.; Chaudhary, K.; Gautam, A.; Kumar, R.; Raghava, G. P. In silico approach for predicting toxicity of peptides and proteins. *PLoS One* **2013**, *8* (9), e73957.
(35) Juba, M.; Porter, D.; Dean, S.; Gillmor, S.; Bishop, B. Characterization and performance of short cationic antimicrobial peptide isomers. *Biopolymers* **2013**, *100* (4), 387−401.
(36) Chen, W.; Yang, B.; Zhou, H.; Sun, L.; Dou, J.; Qian, H.; Huang, W.; Mei, Y.; Han, J. Structure-activity relationships of a snake cathelicidin-related peptide, BF-15. *Peptides* **2011**, *32* (12), 2497−2503.
(37) Zhang, Y.; Zhao, H.; Yu, G. Y.; Liu, X. D.; Shen, J. H.; Lee, W. H. Structure-function relationship of king cobra cathelicidin. *Peptides* **2010**, *31* (8), 1488−1493.
(38) Meyer-Hoffert, U. Neutrophil-derived serine proteases modulate innate immune responses. *Front. Biosci., Landmark Ed.* **2009**, *14*, 3409−3418.
(39) Stromstedt, A. A.; Pasupuleti, M.; Schmidtchen, A.; Malmsten, M. Evaluation of strategies for improving proteolytic resistance of antimicrobial peptides by using variants of EFK17, an internal segment of LL-37. *Antimicrob. Agents Chemother.* **2009**, *53* (2), 593−602.
(40) Dennison, S. R.; Morton, L. H.; Phoenix, D. A. Effect of amidation on the antimicrobial peptide aurein 2.5 from Australian southern bell frogs. *Protein Pept. Lett.* **2012**, *19* (6), 586−591.
(41) Cao, W.; Zhou, Y.; Ma, Y.; Luo, Q.; Wei, D. Expression and purification of antimicrobial peptide adenoregulin with C-amidated terminus in Escherichia coli. *Protein Expression Purif.* **2005**, *40* (2), 404−410.
(42) Torrent, M.; Di Tommaso, P.; Pulido, D.; Nogues, M. V.; Notredame, C.; Boix, E.; Andreu, D. AMPA: an automated web server for prediction of protein antimicrobial regions. *Bioinformatics* **2012**, *28* (1), 130−131.
(43) Eisenberg, D.; Weiss, R. M.; Terwilliger, T. C. The helical hydrophobic moment: a measure of the amphiphilicity of a helix. *Nature* **1982**, *299* (5881), 371−374.

DOI: 10.1021/acs.jmedchem.5b01142
J. Med. Chem. 2015, 58, 8553−8563

(44) Shai, Y.; Oren, Z. Diastereoisomers of cytolysins, a novel class of potent antibacterial peptides. *J. Biol. Chem.* **1996**, *271* (13), 7305−7308.
(45) Papo, N.; Oren, Z.; Pag, U.; Sahl, H. G.; Shai, Y. The consequence of sequence alteration of an amphipathic alpha-helical antimicrobial peptide and its diastereomers. *J. Biol. Chem.* **2002**, *277* (37), 33913−33921.
(46) Gautier, R.; Douguet, D.; Antonny, B.; Drin, G. HELIQUEST: a web server to screen sequences with specific alpha-helical properties. *Bioinformatics* **2008**, *24* (18), 2101−2102.
(47) Rodrigues, M.; Santos, A.; de la Torre, B. G.; Radis-Baptista, G.; Andreu, D.; Santos, N. C. Molecular characterization of the interaction of crotamine-derived nucleolar targeting peptides with lipid membranes. *Biochim. Biophys. Acta, Biomembr.* **2012**, *1818* (11), 2707−2717.
(48) Torrent, M.; de la Torre, B. G.; Nogues, V. M.; Andreu, D.; Boix, E. Bactericidal and membrane disruption activities of the eosinophil cationic protein are largely retained in an N-terminal fragment. *Biochem. J.* **2009**, *421* (3), 425−434.
(49) Mirassou, Y.; Santiveri, C. M.; Perez de Vega, M. J.; Gonzalez-Muniz, R.; Jimenez, M. A. Disulfide bonds versus TrpTrp pairs in irregular beta-hairpins: NMR structure of vammin loop 3-derived peptides as a case study. *ChemBioChem* **2009**, *10* (5), 902−910.
(50) Markley, J. L.; Bax, A.; Arata, Y.; Hilbers, C. W.; Kaptein, R.; Sykes, B. D.; Wright, P. E.; Wuthrich, K. Recommendations for the presentation of NMR structures of proteins and nucleic acids. *J. Mol. Biol.* **1998**, *280* (5), 933−952.
(51) Wuthrich, K. *NMR of Proteins and Nucleic Acids*; John Wiley & Sons: New York, 1986.
(52) Wuthrich, K.; Billeter, M.; Braun, W. Polypeptide secondary structure determination by nuclear magnetic resonance observation of short proton-proton distances. *J. Mol. Biol.* **1984**, *180* (3), 715−740.
(53) Guntert, P. Automated NMR structure calculation with CYANA. *Methods Mol. Biol.* **2004**, *278*, 353−378.
(54) Guntert, P.; Mumenthaler, C.; Wuthrich, K. Torsion angle dynamics for NMR structure calculation with the new program DYANA. *J. Mol. Biol.* **1997**, *273* (1), 283−298.
(55) Cornilescu, G.; Delaglio, F.; Bax, A. Protein backbone angle restraints from searching a database for chemical shift and sequence homology. *J. Biomol. NMR* **1999**, *13* (3), 289−302.
(56) Koradi, R.; Billeter, M.; Wuthrich, K. MOLMOL: a program for display and analysis of macromolecular structures. *J. Mol. Graphics* **1996**, *14* (1), 51−55.
(57) *Methods for dilution antimicrobial susceptibility tests for bacteria that grow aerobically M07-A9*, 9th ed.; Clinical and Laboratory Standards Institute (CLSI): Wayne, PA, 2012.
(58) Wishart, D. S.; Bigam, C. G.; Holm, A.; Hodges, R. S.; Sykes, B. D. 1H, 13C and 15N random coil NMR chemical shifts of the common amino acids. I. Investigations of nearest-neighbor effects. *J. Biomol. NMR* **1995**, *5* (1), 67−81.

DOI: 10.1021/acs.jmedchem.5b01142
J. Med. Chem. 2015, 58, 8553−8563